Energy and Built Environment 4 (2023) 74–85

Contents lists available at ScienceDirect

Energy and Built Environment

journal homepage: http://www.keaipublishing.com/en/journals/energy-and-built-environment/

Experimental investigation of a latent heat thermal energy storage unit encapsulated with molten salt/metal foam composite seeded with nanoparticles

Xin Xiao [a,b,c,*], Hongwei Jia [a], Dongsheng Wen [b], Yousef Golizadeh Akhlaghi [d], Ali Badiei [e]

[a] School of Environmental Science and Engineering, Donghua University, Shanghai, 201620, China
[b] School of Chemical and Process Engineering, University of Leeds, Leeds, LS2 9JT, UK
[c] Shanghai Institute of Pollution Control and Ecological Security, Shanghai, 200092, China
[d] EPSRC National Centre, School of Engineering, Newcastle University, Newcastle, NE4 5TG, UK
[e] School of Engineering, University of Central Lancashire, Preston, PR1 2HE, UK

ARTICLE INFO

Keywords:
Solar salt
Aluminium oxide nanopowder
Metal foam
Heat transfer characteristics

ABSTRACT

Molten salt has been widely used in latent heat thermal energy storage (LHTES) system, which can be incorporated into hybrid photovoltaic/thermal solar system to accommodate the built environment. Solar salt (60 wt.% $NaNO_3$ and 40 wt.% KNO_3) was employed as the phase change materials (PCMs) in this study, and both aluminum oxide (Al_2O_3) nanopowder and metal foam were used to improve the properties of pure solar salt. The synthesis of the salt/metal foam composites seeded with Al_2O_3 nanopowder were performed with the two-step and impregnation methods, and the composite PCMs were characterized morphologically and thermally. Then pure solar salt, the salt/2 wt.% Al_2O_3 nanopowder and salt/copper foam composite seeded with 2 wt.% Al_2O_3 nanopowder were encapsulated in a pilot test rig, respectively, where a heater of 380.0 W was located in the center of the LHTES unit. The charging and discharging processes of the LHTES unit were conducted extensively, whereas the heating temperatures were controlled at 240 °C, 260 °C and 280 °C respectively. Temperature evolutions at radial, angular and axial positions were recorded, and the time-durations and volumetric mean powers during the charging and discharging processes were obtained and calculated subsequently. The results show that physical bonding between Al_2O_3 nanopowder and nitrate molecule has been formed from the morphological pictures together with XRD and FTIR curves. Slight changes are found between the melting/freezing phase change temperatures of the salt/metal foam composites seeded with Al_2O_3 nanopowder and those of pure solar salt, and the specific heats of the salt/Al_2O_3 nanopowder composite slightly increase with the addition of Al_2O_3 nanopowder. The time-duration of the charging process for the salt/copper foam composite seeded with Al_2O_3 nanopowder at the heating temperature of 240 °C can be reduced by about 74.0%, compared to that of pure solar salt, indicating that the heat transfer characteristics of the LHTES unit encapsulated with the salt/copper foam composite seeded with Al_2O_3 nanopowder can be enhanced significantly. Consequently, the mean volumetric powers of the charging process were distinctly enhanced, e.g., the volumetric mean power of heat storage can reach 110.76 kW/m^3, compared to 31.94 kW/m^3 of pure solar salt. However, the additive has little effect on the volumetric mean power of heat retrieval because of the domination of natural air cooling.

1. Introduction

Rapid fossil-fuel depletion and the disturbing environmental pollution coming from fossil-fuel usage make energy as an increasingly important topic. To alleviate energy crisis, considerable attention has been attracted to enabling exploitation of energy from alternative sources such as solar thermal energy and wind energy [1]. Hybrid photovoltaic/thermal (PV/T) solar systems are always used in the Low Carbon and Green Building, so as to accommodate the built environment [2]. The combination of light and thermal storage technology in PV/T system can reduce the constraints of many factors such as season, geography, weather and climate in the conversion process of solar energy as natural renewable energy. Thus solar energy storage has received growing attention, as it is a good solution to store the thermal energy considering the time dependence of solar energy availability [3]. Latent heat thermal energy storage (LHTES) is a proven technology with small temperature

* Corresponding author.
E-mail address: xin.xiao@dhu.edu.cn (X. Xiao).

https://doi.org/10.1016/j.enbenv.2021.08.003
Received 9 May 2021; Received in revised form 6 August 2021; Accepted 6 August 2021
Available online 28 August 2021

Nomenclature

c_p	specific heat (kJ/(kg·K))
d	diameter (m)
E	Energy (kJ/kg)
m	mass (kg)
$\bar{P}$	mean power (kW)
$\bar{P}_V$	volumetric mean power (kW/m^3)
r	Radius (m)
T	temperature (°C)
t	time (s)
V	volume (m^3)
z	position of thermocouple (mm)
Subscript	
c	charging
d	discharging
i	inner
o	outer
PCM	phase change material

variation, which prominently improves the stabilities and efficiencies of energy systems [4].

Molten salts as phase change materials (PCMs) have been considered as storage media in solar energy applications, and widely studied for their moderate phase transition ranges and attractive structural and thermal properties. However, the main issue of molten salt is its low thermo-physical properties such as thermal conductivity and specific heat. Many techniques are addressed the issues of low thermal conductivity and specific heat of pure molten salt such as dispersing nanoparticles into the salt. Nanoparticle with a higher surface energy is dispersed in molten salt, i.e. forming a nano-salt, which maintains the specific heat in most cases. Many researchers measured the thermo-physical properties of nano-salt samples and in most cases apparent improvements were obtained [5–15]. Zhang et al. [5] synthesized the photo-driven PCMs using a sol-gel method, where the microencapsules consider paraffin as the core and Ti_4O_7 nanoparticles-modified SiO_2 as the shells. It was found that the thermal energy storage capacity and thermal conductivity of the microcapsules were greatly enhanced to 169.52 kJ/kg and 1.322 W/(m·K), respectively. Finally the photo-thermal storage efficiency of the microcapsules was up to 85.36%, indicating that the microcapsules were good solar energy storage media in practical applications. Xie et al. [6] investigated the thermal properties of solar salt homogeneously dispersed with graphene nanoplatelets (GNP). It was found that the specific heat increased by 16.7% when the concentration of GNP was 1 wt.%. Navarrete et al. [7] characterized the composite fabricated by solar salt and Al-Cu alloy nano-encapsulated layer. It pointed out that the total energy storage can be increased owing to the contribution of the latent heat storage of the nano-encapsulated PCM. Chieruzzi et al. [8] experimentally studied the thermo-physical properties of nanofluids, which were obtained from solar salt with different mass fractions (0.5 wt.%, 1.0 wt.% and 1.5 wt.%) and types (SiO_2, Al_2O_3 and TiO_2) of nanoparticles. The results indicated that the addition of 1.0 wt.% of nanoparticles into the base salt could increases the specific heats by 15–57% and 1–22% in the solid and liquid phases, respectively. Li et al. [9] extensively studied the specific heats of the molten nano-salt, which was composed of KNO_3-$Ca(NO_3)_2$·$4H_2O$ and SiO_2 nanoparticles with different diameters and mass fractions. When the mass fraction and size of SiO_2 were 1% and 20 nm, respectively, the specific heat of the molten salt nanofluid increased by 17.8%, and the average thermal conductivity increased by 20.2%. Madathil et al. [10] prepared the nanoparticle-incorporated molten salts with KNO_3-$Ca(NO_3)_2$-$LiNO_3$ and MoS_2/CuO nanoparticles, then the thermo-physical properties were systematically investigated. The results revealed that the specific heat and thermal conductivity of the nano-salt with the addition of 0.5 wt.% MoS_2 showed an increment of 20% and 18%, respectively. Seo and Shin [11] studied the influences of SiO_2 nanoparticles with different sizes on the specific heat of ternary nitrate salt eutectic ($LiNO_3$–$NaNO_3$–KNO_3). It was found that the specific heats of the nano-salts were increased by 13–16%, and several nanometer-sized structures were formed by the salt compound around nanoparticles. Tian et al. [12] mixed magnesium (Mg) nanoparticles with ternary salts (Li_2CO_3-$NaCO_3$-K_2CO_3), and studied the microstructures and thermal behaviors of the salt/magnesium composites (CPCM). The ladry leaf-like structure with some curly edges representing the large specific surface area was found in the SEM pictures, and the measured thermal conductivities of CPCM with 0.1–2 wt. % Mg loading were in the range of 1.59–1.93 W/(m·K), indicating about 19.55–45.11% higher than pure ternary salt of 1.33 W/(m·K). Besides the experimental investigations of thermo-physical properties of nano-salts, numerical investigations were also conducted to broaden the research. Hu et al. [13] prepared solar salt-based SiO_2 nanofluids with a lyophilizer, and numerically investigated the heat transfer performances with the Lattice Boltzmann Method (LBM). The results indicated that the specific heat, heat transfer coefficient and Nusselt number could be enhanced by 26.8%, 8.58% and 7.29%, respectively, with 1.0 wt.% SiO_2 nanofluids. Yuan et al. [14] numerically investigated the effects of single-walled carbon nanotubes on specific heat of Li_2CO_3-K_2CO_3, both with Electric Double-Layer modeling and Molecular Dynamics. The results showed that the enhancement of specific heat could be attributed to the increase of the internal energy of the nano-salt ensemble, which was caused by the promotion of the positive and negative charges, and the maximum enhancement of specific heat can be achieved to 19.2%. Hassan and Banerjee [15] developed a machine learning model to predict the specific heats of molten salt seeded with silica, alumina and titania nanoparticles. Multilayer perceptron neural network was used to optimize the features of the model, where the temperature, mass fraction and nominal size of the nanoparticles were considered as the inputs.

However, it can be seen that the thermal conductivities of nano-salts are around 1 W/(m·K), far from the real application of high performance of energy storage. Porous metal foam with abundant specific surface area, attractive mechanical strength and highly-conducting skeletons have been extensively studied to enhance the heat transfer of PCMs [16–24]. Xiao et al. [16] investigated the composite PCMs fabricated by paraffin and copper/nickel foams with different porosities and pore sizes. For copper foam, the results revealed a largest effective thermal conductivity of 16.01 W/(m·K) with 89% porosity and 1.0 mm pore size; for nickel foam, the largest effective thermal conductivity was 2.33 W/(m·K) with 91% porosity and 1.0 mm pore size. Xiao et al. [17] physically mixed 98 wt.% sodium acetate trihydrate (SAT) and 2 wt.% xanthan gum (X) firstly, then the SAT/X composite was impregnated into copper foam (CF) with the saturated mass fraction of 77.2 wt.% using a vacuum impregnation method. The thermal conductivity and latent heat of the SAT/X/CF composite were 176% larger and 5.9% lower, respectively, in comparison with those of pure SAT, while the composites showed good thermal stability after thermal cycling of 200 times. Wang et al. [18] synthesized cetyl palmitate (CP) with binary mixture of 1-hexadecanol (HD) and palmitic acid (PA) and made a series of CP/nickel foam CPCMs. Test results showed that the thermal conductivity of CPCM fabricated by 100 PPI nickel foam could be increased by nearly 5 times, and the thermal stability and reliability of the CPCMs were desirable. Furthermore, the performances of the systems encapsulated with the composite PCMs fabricated by metal foam were also extensively investigated, both with experimental set-ups and numerical models. Zhang et al. [19] experimentally and numerically investigated the heat transfer characteristics of the eutectic salt in a high temperature LHTES unit with and without metal foam. It was found that heat retrieval process dominated by heat conduction was considerably accelerated in the case of eutectic salt/metal foam composite PCM. Wang et al. [20] experimentally investigated the thermal performance of lab-scale shell-and-tube LHTES units for solar energy storage, which were filled with A153 PCMs and homogenous/gradient porosity copper foam. The

results showed that the application of gradient porosity copper foam can reduce the melting time by 37.6%. Cozzolino et al. [21] experimentally studied the thermal behaviour of a tube-in-tank thermal energy system, which was composed of sixteen U-tubes and copper foam impregnated with PureTemp 68. The results indicated that the inlet temperature of the heat transfer fluid (HTF) affected more significantly on the time-duration and peaks magnitude of directional temperature derivative, in comparison with that of the flow rate. Dinesh and Bhattacharya [22] developed a generalized geometry creation model to investigate the effects of foam pore size, pore-to-pore overlap and overall porosity on the melting of PCM and energy absorption. Considering the individual pores of the metal foam, the results indicated that energy storage rate increased with the reduced pore size, and the pore overlap and overall porosity affected energy absorption to some extent. Caliano et al. [23] numerically studied the charging and discharging processes of the biological PCM with and without aluminum foam. The sensitivity study indicated that the temperature range and effective viscosity of mushy zone affected the discharging process apparently. Mousavi et al. [24] numerically studied the effects of PCMs incorporated with copper foam on the performances of a PV/T system. The results showed that the exergy of the PV/T system of PCMs incorporated with copper foam was significantly higher, and the electrical efficiency was enhanced by 2.3%, in comparison with other systems. The addition of metal foam is a good promoter to enhance the PCMs, however, it might decrease the specific heat to some extend, i.e., the storage capacity of the system.

Thus the combination of metal foam and nanoparticles is a good solution to enhance the thermo-physical properties of pure salts or others [25–29]. Ren et al. [26] developed an enthalpy-based immersed boundary-LBM to investigate the melting characteristics of a heat pipe-assisted LHTES unit, which was encapsulated with Li_2CO_3-K_2CO_3 salt enhanced by copper nanoparticles-copper foam. The effectiveness of enhancing the melting characteristics was studied comparatively under various combinations, and it was demonstrated that the enhancement on the thermal performance by inserting metal foam is more effective than that by adding nanoparticle. Mahdi et al. [27–29] developed a compound porous-foam/nanoparticles enhancement technique to significantly improve the melting and freezing processes of the PCM in a triplex-tube heat exchanger, and established a mathematical model considering the non-Darcy effects of porous foam and Brownian motion of nanoparticles.

It can be seen from afore-mentioned studies that majority of the researches focus on the thermo-physical properties of nano-salt in a small scale. Although there are several studies of the heat transfer characteristics of the composite PCMs (PCM with EG or metal foam), a critical action of the experimental investigations of nano-salt needs to be taken forward, that is, the thermal response of the composite PCMs in a LHTES unit. Furthermore, the thermal performances of nano-salt with and without porous media have seldom been reported, it is indispensable to combine the advantages of using nanoparticles and high-porosity metal foams together to enhance the PCMs in LHTES applications. In the present study, aluminium oxide nanopowder (Al_2O_3) were doped into molten solar salt ($NaNO_3$:KNO_3=60:40) solvent with two-step methods firstly, and metal foam was impregnated with the former nano-salt. The morphological and thermal characterization of the composite PCMs were performed with various devices, such as Scanning Electron Microscope (SEM), X-ray diffraction (XRD), Fourier Transform Infrared Spectrometer (FT-IR) and Differential Scanning Calorimeter (DSC). Then solar salt, nano-salt (solar salt seeded with 2 wt.% Al_2O_3 nanopowder) and nano-salt/copper foam composite were considered as the storage media and tested with a pilot experimental rig, which was already used to study the performances of HITEC salt and its composite PCMs preliminarily [30]. The charging and discharging tests were conducted at various heating temperatures. The temperature distributions of the PCMs at different locations were measured, including radial, angular, and axial locations, while the heat transfer characteristics together with the volumetric mean powers of the LHTES unit were revealed extensively.

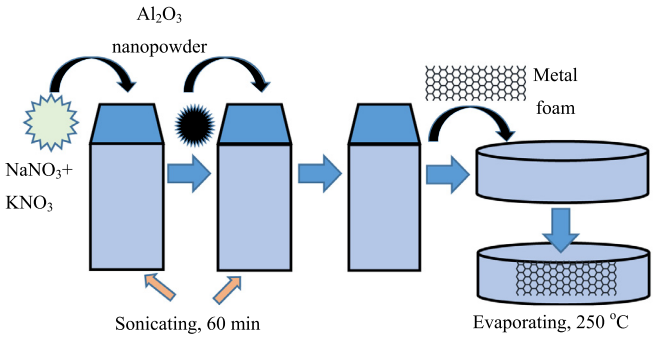

Fig. 1. Synthesized process of salt/metal foam composites seeded with Al_2O_3 nanopowder.

2. Experimental rig and procedure

2.1. Synthesis and characterization of composite PCMs

$NaNO_3$ (Honeywell Fluka, UK) and KNO_3 (Acros Organics, UK) with the purity of 99.0 % were uniformly mixed with the mass ratio of 60:40 to make solar salt. Al_2O_3 nanopowder (40–80 nm APS, Nanostructured & Amorphous Materials Inc., US) and metal foam (Kunshan Jiayisheng Electronics Co. Ltd., CN; porosity: 95.0%; pore size: 10 PPI) were used to improve the thermo-physical properties of pure solar salt. The synthesized process of solar salt/metal foam composites seeded with Al_2O_3 nanopowder was shown in Fig. 1, which is similar to the previous study of HITEC salt/metal foam seeded with Al_2O_3 nanopowder [30]. Solar salt and Al_2O_3 nanopowder with certain mass fractions (1%, 2% or 3%) were wholly dissolved into deionized water to make the solution, which were stirred and sonicated with an ultrasonicator (FB15057; power: 600.0 W; frequency: 37 kHz) for almost one hour. Then nickel/copper foam was physically immersed in the former solution filled in a stainless-steel disc, also with the sonication of 10 min. Subsequently an eurotherm oven (Carbolite Sheffield, UK) was used to heat the final solution at 250 ˚C to evaporate the water and melt the salt, so as to ensure the impregnation process. Finally the disc filled with the salt/metal foam composites seeded with Al_2O_3 nanopowder was taken out and naturally cooled at 30 ˚C for 2 min. The composite PCMs were separated from the disc, and slightly polished.

The morphologies of the composites were characterized by table-top Microscope TM3030Plus (Hitachi High-Technology, Japan). FT-IR Perkin Elmer device (Thermo Scientific, NICOLET iS10) and D8 powder diffractometer (XRD, Bruker, UK) were used as the supplement of the component analysis, including the chemical bonding, molecular structure and degradation effect of the specimens. Infrared light with the wave length between 400 cm^{-1} and 4000 cm^{-1} was transmitted into the specimens, and the transmittance was recorded during the measurement with FT-IR. On the other hand, XRD using Cu-Ka radiation (λ = 1.5418 Å) were performed with the voltage and current of 40 kV and 40 mA, respectively. The specimens were put into the sample holder and scanned over the range from 10 to 60° with a step size 0.035° at total scanning time of 45 min.

To characterize the phase change behaviors of the composite PCMs, all the specimens were undergone the melting–freezing cycles with a Mettler-Toledo DSC (Mettler Toledo Ltd., Leicester, UK). The heating and cooling processes were conducted within 100–300 ˚C at the rates of 5 ˚C/min. The tests were repeated and the average values of three melting-freezing cycles were used to characterize the extrapolated onset temperatures, peak temperatures and latent heats of solar salt, salt/Al_2O_3 nanopowder nanocomposite (nano-salt) and salt/metal foam composite seeded with Al_2O_3 nanopowder. In addition, the specific heats were measured with another heating procedure, that is, isother-

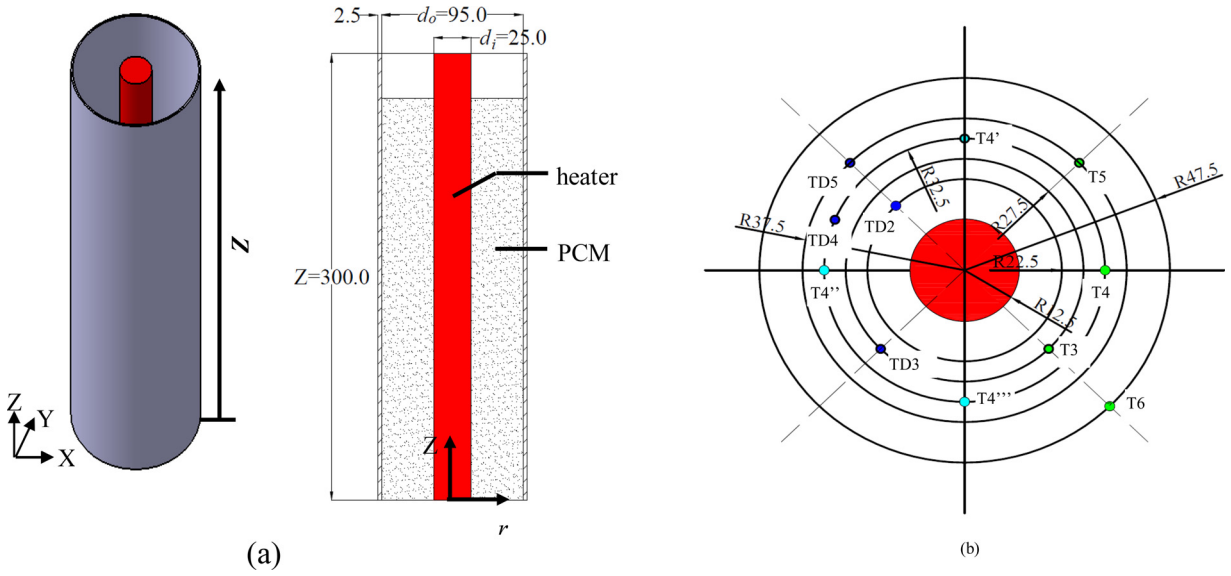

Fig. 2. LHTES unit and the location of thermocouples [30]. (a) LHTES unit (b) thermocouples. (unit: mm).

mal at 100 ˚C for 10 min, heating from 100 ˚C to 300 ˚C with the rate of 25.0 ˚C/min and kept constant at 300 ˚C for 10 min. Then the multiple curving methods were used to calculate the specific heats of the specimen, including empty crucible curve, sapphire curve and specimen curve [31–33], indicating that the calculation was based on those of sapphire already known.

2.2. Experimental test rig set-up

Fig. 2 (a) shows the schematic and section of the cylindric LHTES unit, which was with a height of 300.0 mm and an outer diameter of 100.0 mm. A cartridge heater worked as heat source was located in the inner pipe made of the stainless steel with a diameter of 25.0 mm, while the surroundings were encapsulated with PCMs. The power supplied to the heater was about 380.0 W and conducted by a Varaic connected to the PC, which was via control system using LabVIEW software. Various thermocouples (type K with a diameter of 3.0 mm) with the uncertainty of 0.5 ˚C were inserted at different locations inside the LHTES unit, as shown in Fig. 2 (b). It can be seen that those thermocouples include various radial, angular and axial locations, i.e., the distances from the centre of the heater at radial direction were 22.5 mm, 27.5 mm, 32.5 mm and 37.5 mm, respectively. The thermocouples labelled with *T*D2, *T*D3, *T*D4 and *T*D5 were located in the middle axial positions, i.e., Z = 150 mm, and others labelled with *T*3, *T*4 and *T*5 were located in the lower axial positions, i.e., Z = 125 mm. Additionally, *T*4, *T*4', *T*4'' and *T*4''' located in four angular directions and same axial positions were used to check the homogenous heat transfer of the PCMs. *T*6 in the farthest radial direction were at the deepest point (r = 47 mm, Z = 25 mm). In order to minimize the heat loss of the LHTES unit, the unit was fully covered with multi-layer thermal insulation and radiant shielding (aluminium fibre) materials. Because of the safety requirement during melting of salt, a safety pressure relief valve was added to ensure that no pressure was built up inside the unit.

2.3. Experimental procedure and uncertainty analysis

The LHTES unit was filled with solar salt, salt/2 wt. % Al_2O_3 nanopowder nanocomposite (nano-salt), salt/copper foam composite seeded with 2 wt. % Al_2O_3 nanopowder (nano-salt/copper foam composite), respectively. In order to accommodate the thermal expansion of pure solar salt, only 90.0 vol.% of the LHTES unit was filled with pure solar salt, i.e., the amount in three cases were 2500 g, and 2250 g and 2000 g, respectively. As a result, the nano-salt and nano-salt/copper foam composite encapsulated in the LHTES unit were 2295 g and 2676 g, respectively.

The charging experiments were conducted with the controlled heating temperatures set at 240 ˚C, 260 ˚C and 280 ˚C for solar salt and its composites, respectively, when the entire LHTES unit was initially at a room temperature of 10–30 ˚C. During the charging process, the controlled heating temperature represents the maximum value of thermocouple *T*5, which increases slightly because of the heater. As a result, the heater is stopped working when *T*5 reaches the controlled heating temperature such as 240 ˚C, 260 ˚C or 280 ˚C, respectively. The discharging experiments were started after the LHTES unit mainly reached the heating temperatures, and the whole unit was cooled down naturally at a surrounding temperature of about 10–20 ˚C subsequently. The variation of the surrounding temperature was caused by the temperature fluctuation of the ventilating cabine. In the meantime, the temperature evolutions of all thermocouples were instantly recorded with a time interval of 1.4 s once the tests were performed, where the interval was determined by a program in Labview software. Similarly, the temperature evolutions during the charging and discharging processes were presented under the second thermal cycle, as a first thermal cycle was made to remove the air in salt powder.

In the present study, the uncertainty of the temperature evolution was determined to be 2.02% using the uncertainty propagation analysis. Considering the uncertainties of the mass of the PCM, the specific heat of the PCM and the time-duration were 0.5%, 0.5% and 1.0%, respectively, the overall uncertainty of the volumetric mean power was determined to be 2.36% with the following formula.

$$\frac{\delta \bar{P}_V}{\bar{P}_V} = \sqrt{\left(\frac{\delta m}{m}\right)^2 + \left(\frac{\delta c_p}{c_p}\right)^2 + \left(\frac{\delta T}{T}\right)^2 + \left(\frac{\delta t}{t}\right)^2} \quad (1)$$

2.4. Volumetric mean power

Similarly to the previous studies [30,33], the specific heats of pure salt and composite PCMs were taken as a function of the temperature [33], and the apparent specific heat integrated with latent heat accounting for the phase change process was adopted in the present study. Because the summation of the latent and sensible energy stored by the PCMs indicated the energy absorbed by the LHTES unit, the apparent specific heat together with the mass of the PCMs were used to determine the total energy. Thus the energy and volumetric mean powers of

the LHTES unit during the charging process were calculated as follows, respectively:

$$E_c = m_{PCM} \int_{40}^{T_{heating}} c_{p,PCM}\, dT \tag{2}$$

$$\bar{P}_{V-c} = \frac{E_c}{t_c V} \tag{3}$$

where t_c denotes the time-duration of heat storage from 40 ˚C to the heating temperatures, V denotes the volume of the LHTES unit. The energy and volumetric mean powers of the LHTES unit during the discharging process were calculated as follows, respectively:

$$E_d = m_{PCM} \int_{T_{end}}^{T_{heating}} c_{p,PCM}\, dT \tag{4}$$

$$\bar{P}_{V-d} = \frac{E_d}{t_d V} \tag{5}$$

where t_d denotes the time-duration of heat retrieval from the heating temperatures to the end temperatures, indicating an adjustment as the initial temperatures during the discharging process were a little larger than the controlled heating temperatures. Furthermore, in order to understand the optimal temperature difference between the end and surrounding temperatures for the real application, the end temperatures during the discharging process were set at 50 ˚C, 100 ˚C and 150 ˚C, respectively.

3. Results and discussion

3.1. Morphology and thermal characteristics of composite PCMs

Fig. 3 shows the SEM images of salt/2 wt.% Al_2O_3 nanocomposite, salt/nickel foam composite seeded with 2 wt.% Al_2O_3 nanopowder and salt/copper foam composite seeded with 2 wt.% Al_2O_3 nanopowder. The rugged surface in Fig. 3 (a) was caused by the shrinkage of salt during freezing, because the density of solar salt in solid state is larger than that in liquid state. However, the phenomenon of the shrinkage is not obvious in Fig. 3 (b) and (c). The possible reason is that metal foam can provide good supporting for the nanocomposites. Normally, Al_2O_3 nanopowder can mix well with the salt, and the salt/Al_2O_3 nanocomposites are totally compatible with metal foam.

Fig. 4 shows the XRD and FT-IR analyses of solar salt, salt/Al_2O_3 nanocomposites and salt/metal foam composite seeded with Al_2O_3 nanopowder, which can determine the crystal structures of the materials. It can be seen from XRD analysis in Fig. 4 (a) that pure salt and all composite PCMs have no obvious difference of intensity peaks. With the addition of metal foam, several extra characteristic peaks are generated on the surface as shown in the rectangular region. However, the characteristic peaks shows no significant change with the addition of Al_2O_3 nanopowder, which is believed to be due to the formation of the physical bonding between Al_2O_3 nanopowder and nitrate molecule during the synthesis process. It can be seen from Fig. 4 (b) that the FT-IR absorption spectra are practically the same for all the specimens, indicating that the existence of the physical bonding of Al_2O_3 nanopowder with nitrate molecule inherently does not disturb the chemical structure interaction for chemical stability.

Fig. 5 shows the variations of the phase change temperatures of solar salt, salt/Al_2O_3 nanocomposite and salt/metal foam composite seeded with Al_2O_3 nanopowder. The addition of Al_2O_3 nanopowder slightly affects the phase change temperatures of pure solar salt, with the maximum deviation of the peak melting/freezing phase change temperatures of 0.68 ˚C. The combined effects of Al_2O_3 nanopowder and metal foam induce the variation of phase change temperatures of the salt/metal foam composites seeded with 2 wt.% Al_2O_3 nanopowder, e.g., the extrapolated onset melting temperature of the salt/copper foam composite seeded with 2 wt.% Al_2O_3 nanopowder shifts from 220.82 ˚C to 217.30 ˚C, while the extrapolated onset freezing temperature shifts from 227.45 ˚C to 230.06 ˚C, compared with those of solar salt. The early occurrence of phase change can be attributed to the good combination and dispersion performance of the salt and nanoparticles/metal foam, and the promotion of the good thermo-physical properties of nanoparticles and metal foam.

Fig. 6 shows the examples of the apparent specific heats of solar salt, salt/Al_2O_3 nanocomposites, salt/metal foam composites seeded with Al_2O_3 nanopowder, which will be used to calculate the energy and mean power of the LHTES unit. Table 1 also lists the specific heats of solar salt and composite PCMs. It can be seen that the specific heats of the nano-salts slightly increase with the addition of Al_2O_3 nanopowder in solid state, in comparison with that of pure salt. However, the specific heats of the salt/metal foam composites apparently decrease as the specific heats of nickel or copper are lower than that of pure salt. As a result, because of the addition of Al_2O_3 nanopowder, the specific heats of the salt/metal foam composites seeded with Al_2O_3 nanopowder show with slight increment, compared to those of the salt/metal foam composites, e.g., the specific heat of the salt/copper foam composite seeded with 2 wt.% Al_2O_3 nanopowder is 1.6895 kJ/(kg·˚C), while that of the salt/copper foam composite is 1.5921 kJ/(kg·˚C). The reason is due to the nanometer-sized structure formed by the salt compound around Al_2O_3 nanopowder, which amplifies the effect of surface energy on the effective specific heat [35]. Furthermore, considering the longer period of the sensible heat storage for solar salt (usually from room temperature to 200 ˚C), the sample with the addition of 2 wt.% Al_2O_3 nanopowder which has the largest specific heat in solid state will be used as the study object in the following systematic tests.

3.2. Diverse controlled heating temperatures

Fig. 7 shows the temperature evolutions for pure solar salt at different heating temperatures. The charging process can be accelerated with the higher controlled heating temperature, e.g., the charging times are 14938 s and 9002 s at the heating temperatures of 260 ˚C and 280 ˚C, respectively. This is due to large temperature difference between the PCMs and inner heater leads to the enhanced heat transfer. The lower temperature of point *T*6 shown in elliptical regions in Fig. 7 is due to the contact with the lateral surface of the LHTES unit, which causes heat loss from the lateral surface of the LHTES unit accordingly.

It can be seen from Fig. 7(I) that thermocouples at $Z = 150$ mm (*TD*3, *TD*4 and *TD*5) show a higher melting characteristics than $Z = 125$ mm (*T*3, *T*4 and *T*5), e.g. the temperatures of *T*3, *T*4 and *T*5 are 192.52 ˚C, 176.82 ˚C and 176.86 ˚C, respectively, while those of *TD*3, *TD*4 and *TD*5 are 214.29 ˚C, 207.96 ˚C and 204.58 ˚C at the heating temperature of 260 ˚C and time of 5000 s. The heat transfer depends on the conduction at the starting period, then natural convection appears as soon as the phase change starts. The buoyancy effect induced by the gravity would result in the higher melting characteristics of points *TD*3, *TD*4 and *TD*5. There are slight differences among *T*4, *T*4', *T*4'' and *T*4''', as shown in rectangular regions in Fig. 7(I). Those minor differences could be attributed to the following reasons. On one hand, the shrinkage of PCMs during freezing might cause several cavities inside the PCMs region, inducing the temperature difference during the charging process while the salt is still in solid state. However, the temperatures of *T*4, *T*4', *T*4'' and *T*4''' are almost the same while the salt is totally in liquid state. On the other hand, the positions of the four thermocouples might not be at the exact radial and axial positions, slightly affecting the comparisons among those test points. In general, the heat transfer seems homogenous at the same radial and axial positions.

Fig. 7(II) shows the temperature evolutions during the discharging process. The whole process is very slow, and a flat region at about 100 ˚C represent the solid-solid phase change. The discharging times are about 42574 s and 42003 s when the starting temperatures are 260 ˚C and 280 ˚C, respectively. On one hand, the natural air cooling outside the LHTES unit dominated the whole process induce large thermal resis-

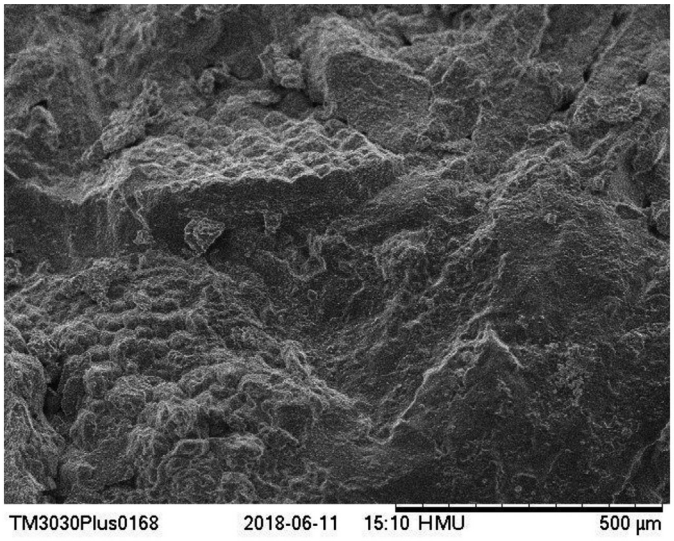

(a)

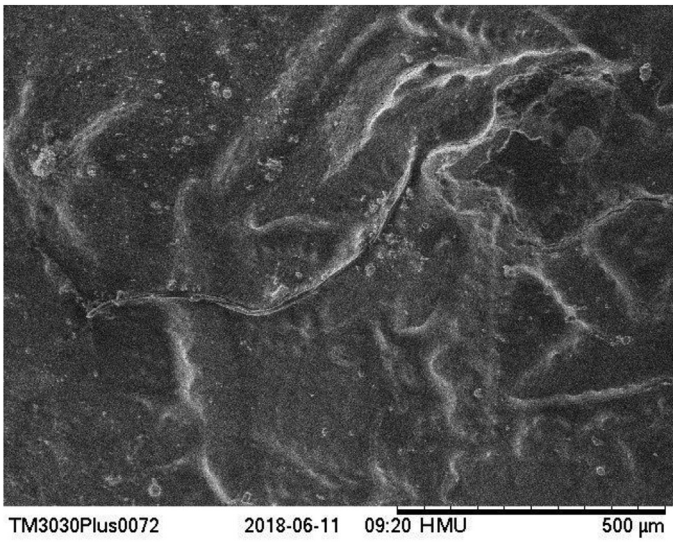

(b)

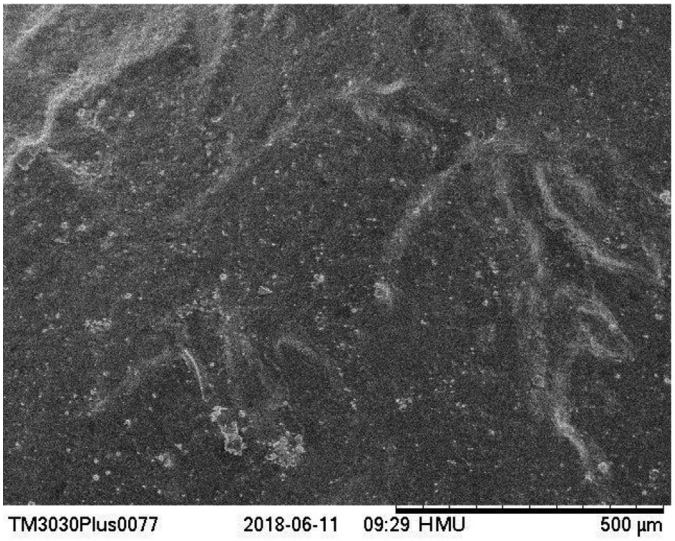

(c)

Fig. 3. SEM images of solar salt/Al_2O_3 nanopowder with and without metal foam. (a) salt/2 wt.% Al_2O_3 nanopowder [34] (b) salt/nickel foam composite seeded with 2 wt. % Al_2O_3 nanopowder (c) salt/copper foam composite seeded with 2 wt.% Al_2O_3 nanopowder.

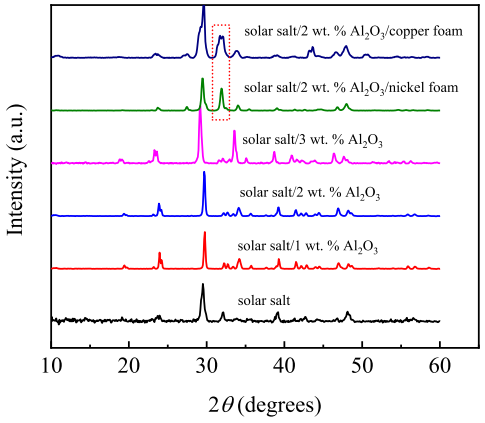

(a)

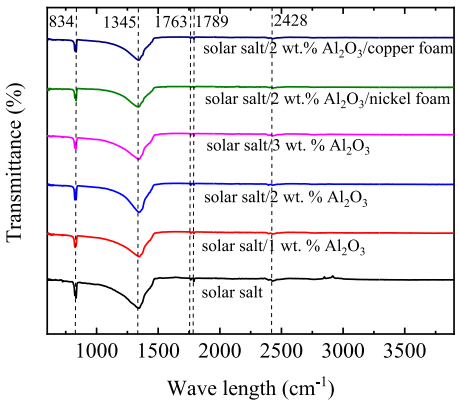

(b)

Fig. 4. XRD (a) and FT-IR (b) analyses of solar salt and composite PCMs.

Table 1
Specific heats of solar salt and composite PCMs.

Specific heat (kJ/(kg·°C))	Solar salt	+Al_2O_3			Solar salt/nickel foam	Solar salt/copper foam	Solar salt /2 wt.% Al_2O_3/nickel foam	Solar salt /2 wt.% Al_2O_3/copper foam
		1 wt.%	2 wt.%	3 wt.%				
Solid state (150-200 °C)	1.8300	1.8532	1.8622	1.7986	1.7215	1.5921	1.7284	1.6895
Liquid state (260-290 °C)	1.6765	1.5586	1.5440	1.6487	1.5674	1.4391	1.5324	1.4879

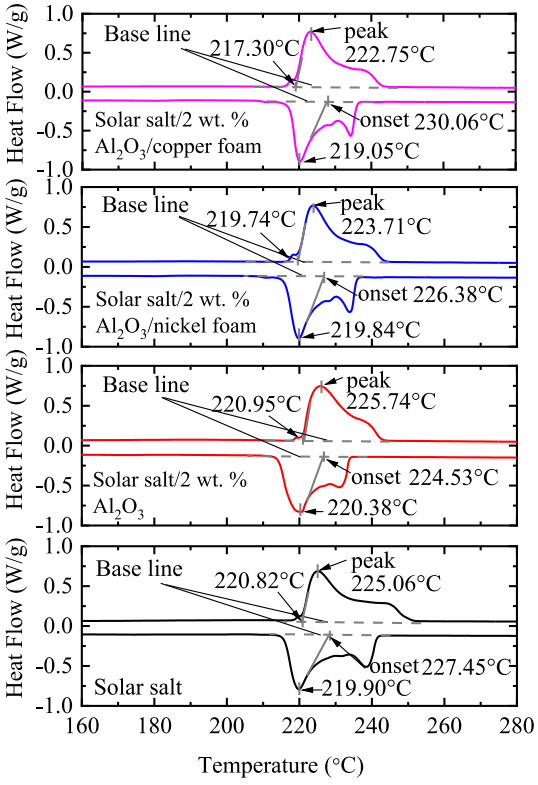

Fig. 5. DSC curves of solar salt and composite PCMs.

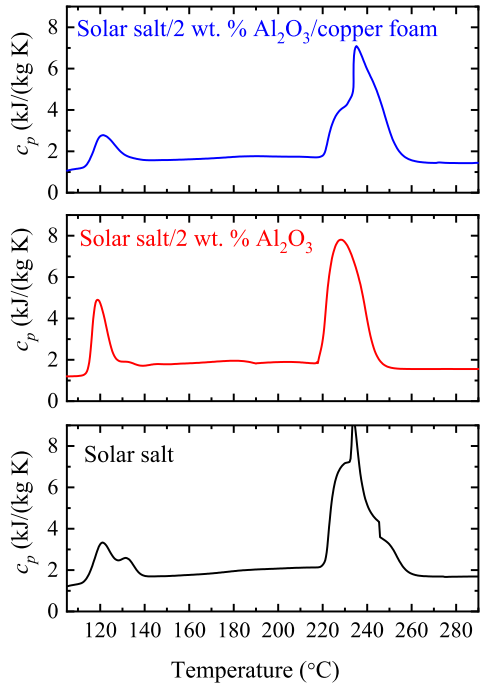

Fig. 6. Apparent specific heats of solar salt and composite PCMs.

tance. On the other hand, the fluctuation of the inner temperature of the ventilating cabin in the lab would slightly affect the discharging process.

3.3. Comparison of pure salt and composite PCMs

The temperature evolutions and distributions of solar salt and composite PCMs are shown in Fig. 8, both for the charging and discharging processes. It can be seen from Fig. 8 (a-I) and (a-II) that the temperature of *TD*3, *TD*4 and *TD*5 increase more quickly than those of *T*3, *T*4 and *T*5 respectively, which are caused by natural convection of pure salt as *TD*3, *TD*4 and *TD*5 are above and with the same radial and different axial positions. With the addition of Al_2O_3 nanopowder and copper foam, the temperature could raise faster, e.g., the temperatures for *TD*4 are 166.55 °C, 214.86 °C, 235.60 °C at 3000 s for pure solar salt, salt/2 wt.% Al_2O_3 nanopowder and salt/copper foam composite seeded with 2 wt.% Al_2O_3 nanopowder, respectively. Only the temperatures of thermocouples above 50 °C in the discharging process are shown in Fig. 8(b). The discharging process is relatively slow as natural air cooling dominates the whole process, which induces large thermal resistance. Furthermore, it can be seen that slight difference appears between *T*3, *T*4, *T*5 and *TD*3, TD4, TD5 during the whole discharging process.

If points *T*3, *T*4 and *T*5 are chosen as the representative thermocouples, a detailed comparison of temperature evolutions and distributions of solar salt and composite PCMs is shown in Fig. 9. As the phase change temperature of solar salt is about 220 °C shown in Fig. 5, the heat conduction dominates a large portion of the whole charging process when the controlled heating temperature is 240 °C. As a result, the temperature of *T*3 increases more quickly than those of *T*4 and *T*5 for all three kinds of materials. However, there is no obvious difference between *T*4 and *T*5, especially for pure solar salt and salt/2 wt.% Al_2O_3 nanopowder. The possible reason is that points *T*4 and *T*5 is far from the inner heater, and natural convection appears to some extent during melting of solar salt. In addition, temperature of *T*4 increases a little slower than that of *T*5 for the salt/copper foam composite seeded with 2 wt.% Al_2O_3 nanopowder, which is due to the high conductive property of copper skeleton. In all, the improvements in temperature distributions over time mainly attribute to the enhancement of the thermal conductivity of the composite PCMs. It can be seen from Fig. 9(a) that the time-durations of the salt/2 wt.% Al_2O_3 nanopowder, salt/copper foam composite seeded with 2 wt.% Al_2O_3 nanopowder for heat storage are considerably reduced. The charging times are 18011 s, 11760 s and 4683 s for solar salt, salt/2 wt.% Al_2O_3 nanopowder, salt/copper foam composite seeded with 2 wt.% Al_2O_3 nanopowder, indicating a reduction of the time-duration by 34.7% and 74.0% for nano-salt and nano-salt/copper foam composite, respectively. The considerable enhancement is similar to the previous research [19]. However, the discharging times are 38276 s, 34324 s and 40551 s for solar salt, salt/2 wt.% Al_2O_3 nanopowder, salt/copper foam composite seeded with 2 wt.% Al_2O_3 nanopowder, respectively (T_{end}=50 °C). It is unusual that although the thermo-properties of the composite PCMs are enhanced by the additives, the discharging process did not be accelerated as expected, which is mainly due to the reason that natural air cooling with large thermal resistance

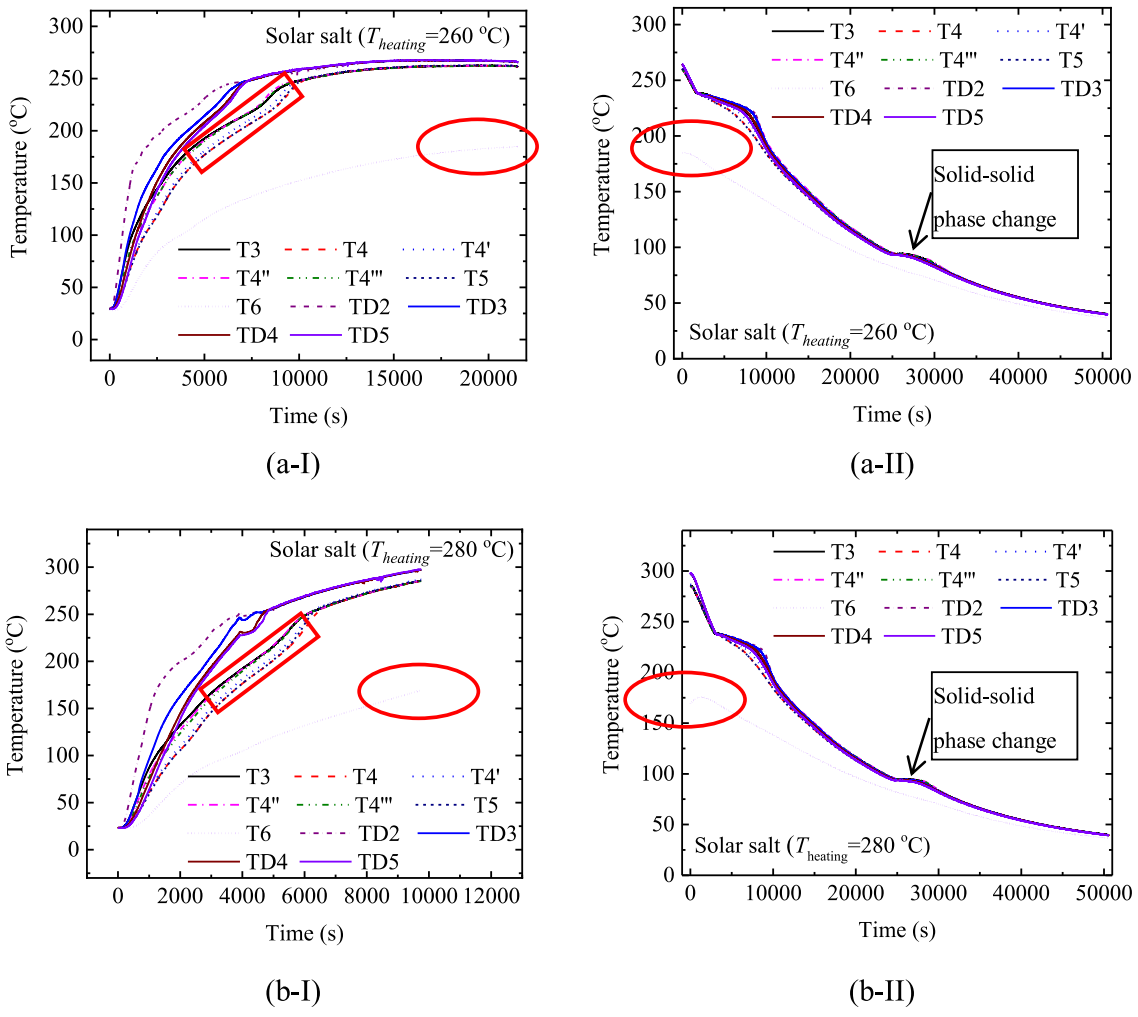

Fig. 7. Temperature evolutions and distributions of solar salt at different heating temperatures (I: heat storage; II: heat retrieval). (a) 260 °C (b) 280 °C.

outside the LHTES unit dominated the whole process. Furthermore, on one hand, as shown in Fig. 8 (a-III) and (b-III), the LHTES unit with the salt/copper foam composite seeded with 2 wt.% Al_2O_3 nanopowder can achieve the higher temperature after the charging process, inducing the slightly larger time-duration to release the heat. On the other hand, the experiments of pure solar salt and salt/2 wt.% Al_2O_3 nanopowder were conducted at the surrounding temperatures of about 13–15 °C, and that of salt/copper foam composite seeded with 2 wt.% Al_2O_3 nanopowder was conducted at the surrounding temperatures of about 16–18 °C, because of the variation of the inner temperature of the ventilating cabin in the lab.

3.4. Power rate during heat storage/retrieval

The energy stored includes the sensible and latent heats. The latent heat is incorporated into the specific heat of PCM, which is named apparent specific heat accounting for the phase change process [30], as shown in Fig. 6. Based on the mass and apparent specific heat of the PCMs encapsulated in the LHTES unit, the heat storage and retrieval energies were approximately achieved, as shown in Fig. 10. It can be seen from Fig. 10 (a) that obviously different energy amounts can be stored with various PCMs, and the energy stored by solar salt is slightly larger than that of the composite PCMs, e.g., when the heating temperature is 280 °C, the energy stored by the salt/copper foam composite seeded with 2 wt.% Al_2O_3 nanopowder is about 1177 kJ, compared to that of solar salt of 1271 kJ. It should be noted that the energy stored is a little larger due to the large mass of the salt/copper foam composite seeded with 2 wt.% Al_2O_3 nanopowder, in comparison with that of the salt/2 wt.% Al_2O_3 nanocomposite. In addition, as shown in Fig. 10 (b), the energy retrieval amounts are apparently different from various end temperatures, e.g., when the end temperature are 50 °C, 100 °C and 150 °C, respectively, the energy released by the salt/copper foam composite seeded with 2 wt.% Al_2O_3 nanopowder are 1155 kJ, 1043 kJ and 816 kJ at heating temperature of 280 °C.

The volumetric mean powers were achieved by considering the time-durations of the charging and discharging processes. Fig. 11 and Table 2 show the volumetric mean powers of heat storage and retrieval for solar salt and composite PCMs. It can be seen that the volumetric mean powers of heat storage in the LHTES unit are in the range of 31.94–187.00 kW/m^3, considering different heating temperatures and PCMs. While the volumetric mean powers of heat retrieval from the LHTES unit are in the range of 12.48–16.73 kW/m^3, 21.86–28.34 kW/m^3 and 29.19–35.08 kW/m^3 when the end temperatures are 50 °C, 100 °C and 150 °C, respectively.

It can be seen from Fig. 11 that the volumetric mean powers of the LHTES unit during the charging process are significantly enhanced by involving the application of the composite PCM, e.g., the volumetric mean power for the salt/copper foam composite seeded with 2 wt.% Al_2O_3 nanopowder at the heating temperature of 280 °C increases to 109.32 kW/m^3, in comparison with 53.01 kW/m^3 of pure solar salt. However, the volumetric mean powers during the discharging process are quite irregular, as slight difference exists among various PCMs. The

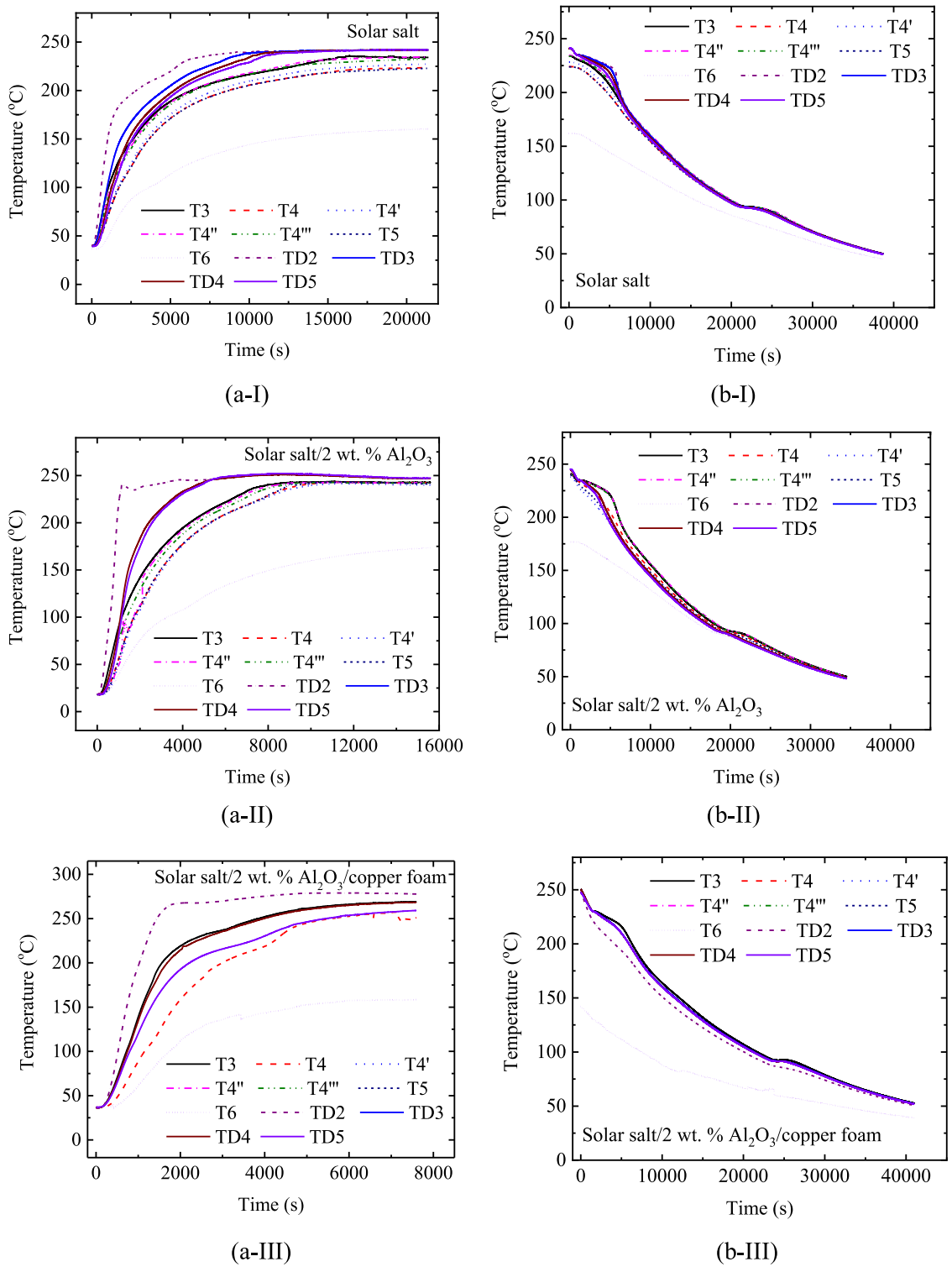

Fig. 8. Temperature evolutions and distributions of solar salt and composite PCMs ($T_{heating}$=240 °C). (a) heat storage (b) heat retrieval. I, II, III marks represent solar salt, solar salt/2 wt. % Al_2O_3 nanopowder and solar salt/copper foam composite seeded with 2 wt.% Al_2O_3 nanopowder, respectively.

reason is that the whole process is dominated by natural air cooling which causes longer discharging process. In addition, it can also be seen from Fig. 11 and Table 2 that the volumetric mean powers of heat retrieval for the salt/copper foam composite seeded with 2 wt.% Al_2O_3 nanopowder at the heating temperature of 280 °C are 15.14 kW/m^3, 25.56 kW/m^3 and 33.03 kW/m^3 when the end temperatures are 50 °C, 100 °C and 150 °C, respectively. The volumetric mean power of heat retrieval decreases with the descending of the end temperature, mainly because of the apparent decrease of the time-duration in comparison with the reduction of released energy. The heat transfer between the LHTES unit and surrounding is affected by the temperature difference between them, and it becomes very slow if the temperature difference

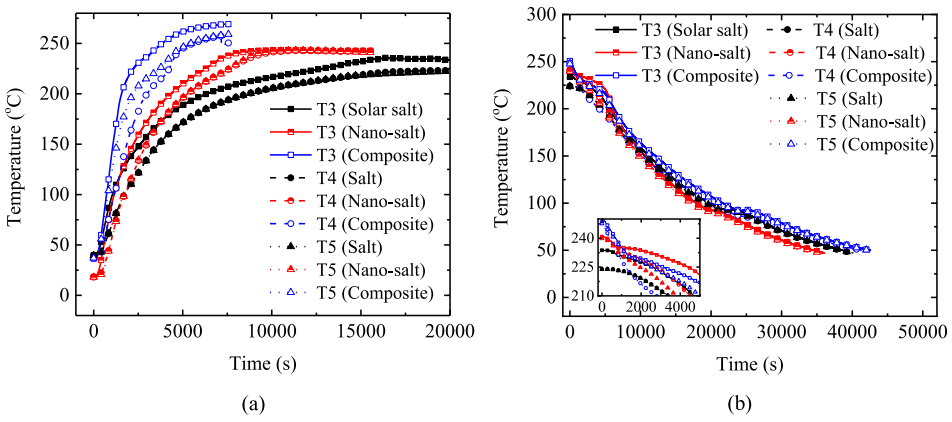

Fig. 9. Comparison of temperature evolutions and distributions of solar salt and composite PCMs ($T_{heating}$=240 °C). (a) heat storage (b) heat retrieval. The closed, half-open and open marks represent solar salt, solar salt/2 wt. % Al_2O_3 nanopowder and solar salt/copper foam composite seeded with 2 wt. % Al_2O_3 nanopowder, respectively.

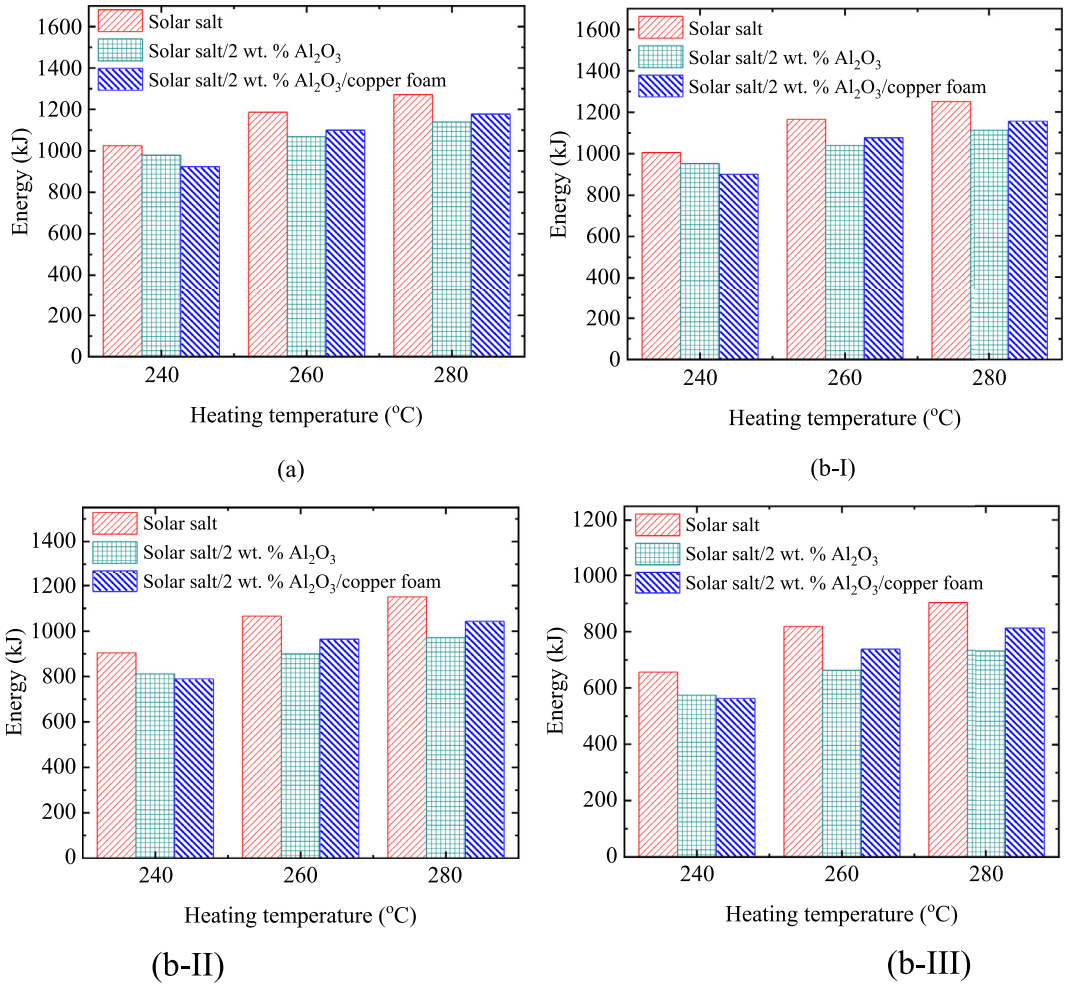

Fig. 10. Energies of heat storage and retrieval for solar salt and composite PCMs. (a) Heat storage (b) Heat retrieval, I: T_{end}=50 °C, II: T_{end}=100 °C, III: T_{end}=150 °C.

as the driving force is small. However, the increase of the volumetric mean power causes the reduction of the usable energy, thus a suitable end temperature should be considered in real application.

4. Conclusions

In the present study, the composite PCMs with nanoparticles and porous metal foam were synthesized and extensively characterized, then the charging and discharging characteristics of a pilot test rig were experimentally investigated, which was encapsulated with solar salt, salt/2 wt. % Al_2O_3 nanopowder (nano-salt) and salt/copper foam composite seeded with 2 wt. % Al_2O_3, respectively. The following conclusions can be drawn:

1) Both Al_2O_3 nanopowder and metal foam can mix well with pure solar salt. The presence of Al_2O_3 nanopowder and porous metal foam made the phase change temperatures shift slightly. The specific heats of the nano-salts are apparently enhanced with the addition of Al_2O_3 nanopowder both in solid and liquid states.
2) The heat transfer seems homogenous at the same radial and axis positions of the LHTES unit. Both Al_2O_3 nanopowder and copper foam

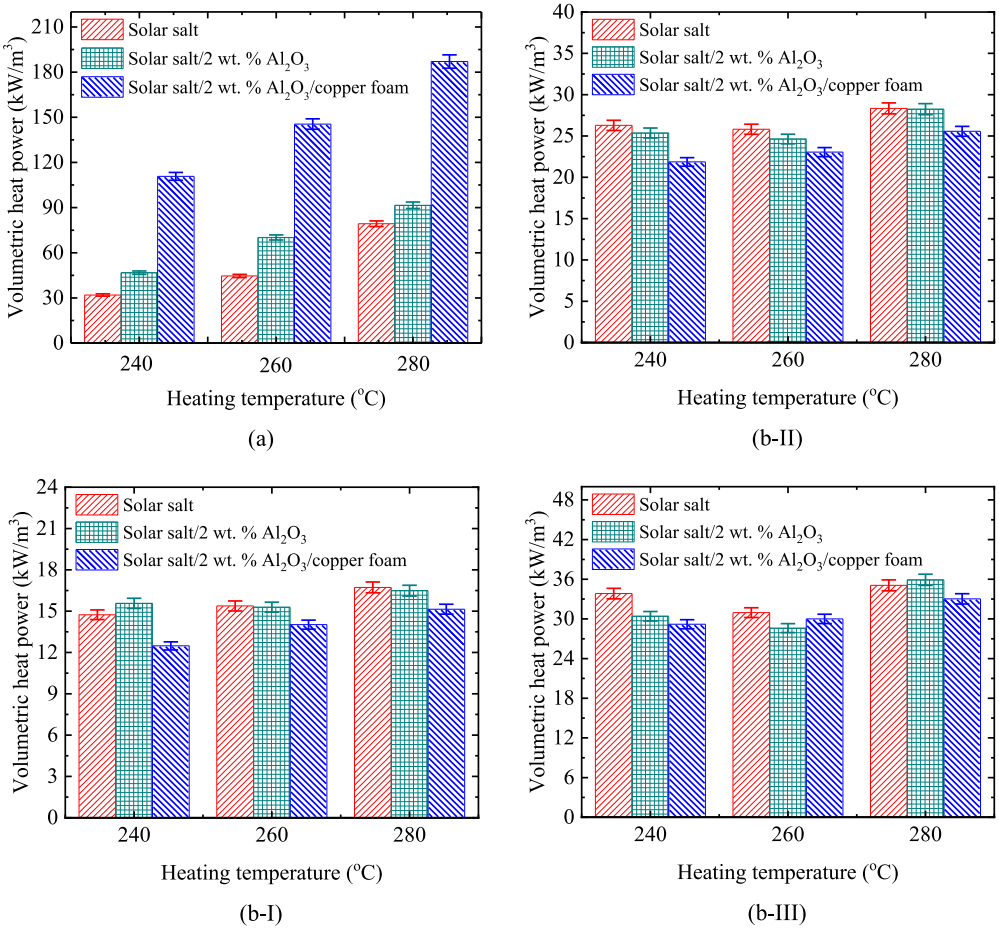

Fig. 11. Volumetric mean powers of heat storage and retrieval for solar salt and composite PCMs. (a) Heat storage (b) Heat retrieval, I: T_{end}=50 ˚C, II: T_{end}=100 ˚C, III: T_{end}=150 ˚C.

Table 2
Volumetric mean powers of heat storage and retrieval for pure salt and composite PCMs.

$\bar{P}_V$ (kW/m^3)		Pure solar salt	Salt/2 wt.% Al_2O_3 nanopowder	Salt/copper foam composite seeded with 2 wt.% Al_2O_3 nanopowder
Volumetric mean power of heat storage	$T_{initial}$=40 ˚C, T_{end}=240°C	31.94	46.77	110.76
	$T_{initial}$=40 °C, T_{end}=260°C	44.59	70.19	145.49
	$T_{initial}$=40 ˚C, T_{end}=280°C	79.29	91.54	187.00
Volumetric mean power of heat retrieval	$T_{initial}$=240 °C, T_{end}=50°C	14.74	15.57	12.48
	$T_{initial}$=260 ˚C, T_{end}=50°C	15.38	15.29	14.02
	$T_{initial}$=280 °C, T_{end}=50°C	16.73	16.49	15.14
	$T_{initial}$=240 ˚C, T_{end}=100°C	26.29	25.36	21.86
	$T_{initial}$=260 °C, T_{end}=100 °C	25.81	24.64	23.05
	$T_{initial}$=280 ˚C, T_{end}=100°C	28.34	28.25	25.56
	$T_{initial}$=240 °C, T_{end}=150°C	33.83	30.41	29.19
	$T_{initial}$=260 ˚C, T_{end}=150°C	30.95	28.61	30.01
	$T_{initial}$=280 °C, T_{end}=150°C	35.08	35.91	33.03

can significantly improve the heat transfer of pure solar salt, e.g., the time-duration of heat storage at the controlled heating temperature of 240 ˚C can be reduced by 34.7% and 74.0% for nano-salt and nano-salt/copper foam composite, respectively. The additives can slightly decrease the time-duration of heat retrieval because natural air cooling dominates the process.

3) The volumetric mean powers of heat storage in the LHTES unit are in the range of 31.94–187.00 kW/m^3, whereas the volumetric mean powers of heat retrieval from the LHTES unit range from 12.48 kW/m^3 to 16.73 kW/m^3. The volumetric mean powers of heat storage can be significantly improved, e.g., the volumetric mean power of the salt/copper foam composite seeded with 2 wt.% Al_2O_3 nanopowder at the heating temperature of 280 ˚C increases to 109.32 kW/m^3, compared to 53.01 kW/m^3 of pure solar salt.

CRediT authorship contribution statement

X. Xiao, conceptualization, investigation, writing, original draft preparation, review and editing, funding acquisition
H. W. Jia, investigation
D. S. Wen, project administration
Y.G. Akhlaghi, review and editing
A. Badiei, review and editing

Declaration of Competing Interest

The authors declare that they have no known competing financial interests or personal relationships that could have appeared to influence the work reported in this paper.

Acknowledgements

This research has received funding from the Shanghai Pujiang Program (No. 20PJ1400200), the Shanghai overseas high level Talents Program, the Fundamental Research Funds for the Central Universities of China (No. 2232021D-11&2232018D3-37), European Union's Horizon 2020 research and Innovation Programme under the Marie Sklodowska-Curie grant (No. 706788), and the Natural Science Foundation of China (No. 52006030). The authors would like to extend their acknowledgement to Dr. Afrah Awad and Mr. Hailong Ma for the kind help.

References

[1] GJ Nathan, M Jafarian, BB Dally, WL Saw, PJ Ashman, E Hu, A. Steinfeld, Solar thermal hybrids for combustion power plant: a growing opportunity, Prog Energ Combust 64 (2018) 4–28.
[2] NR Darghouth, G Barbose, J Zuboy, PJ Gagnon, AD Mills, L. Bird, Demand charge savings from solar PV and energy storage, Energy Policy 146 (2020) 111766.
[3] S Kuravi, J Trahan, DY Goswami, MM Rahman, EK. Stefanakos, Thermal energy storage technologies and systems for concentrating solar power plants, Prog Energ Combust 39 (2013) 285–319.
[4] HY Gao, JJ Wang, X Chen, G Wang, XB Huang, A Li, WJ. Dong, Nanoconfinement effects on thermal properties of nanoporous shape-stabilized composite PCMs: a review, Nano Energy 53 (2018) 769–797.
[5] Y Zhang, XY Li, JQ Li, CY Ma, LJ Guo, XM. Meng, Solar-driven phase change microencapsulation with efficient Ti_4O_7 nanoconverter for latent heat storage, Nano Energy 53 (2018) 579–586.
[6] QZ Xie, QZ Zhu, Y. Li, Thermal storage properties of molten nitrate salt-based nanofluids with graphene nanoplatelets, Nanoscale Res. Lett. 11 (2016) 306.
[7] N Navarrete, R Mondragon, DS Wen, ME Navarro, YL Ding, J Enrique Julia, Thermal energy storage of molten salt - based nanofluid containing nano-encapsulated metal alloy phase change materials, Energy 167 (2019) 912–920.
[8] M Chieruzzi, GF Cerritelli, A Miliozzi, JM. Kenny, Effect of nanoparticles on heat capacity of nanofluids based on molten salts as PCM for thermal energy storage, Nanoscale Res. Lett. 8 (2013) 448.
[9] Y Li, X Chen, YT Wu, YW Lu, RP Zhi, X Wang, CF. Ma, Experimental study on the effect of SiO_2 nanoparticle dispersion on the thermophysical properties of binary nitrate molten salt, Sol Energy 183 (2019) 776–781.
[10] PK Madathil, N Balagi, P Saha, J Bharali, PVC Rao, NV Choudary, K Ramesh, Preparation and characterization of molten salt based nanothermic fluids with enhanced thermal properties for solar thermal applications, Appl. Therm. Eng. 109 (2016) 901–905.
[11] JH Seo, DH. Shin, Size effect of nanoparticle on specific heat in a ternary nitrate ($LiNO_3$–$NaNO_3$–KNO_3) salt eutectic for thermal energy storage, Appl. Therm. Eng. 102 (2016) 144–148.
[12] HQ Tian, LC Dua, XL Wei, SY Deng, WL Wang, J. Ding, Enhanced thermal conductivity of ternary carbonate salt phase change material with Mg particles for solar thermal energy storage, Appl. Energy 204 (2017) 525–530.
[13] YW Hu, YR He, HD Gao, ZD. Zhang, Forced convective heat transfer characteristics of solar salt-based SiO_2 nanofluids in solar energy applications, Appl. Therm. Eng. 155 (2019) 650–659.
[14] F Yuan, MJ Li, Y Qiu, Z Ma, MJ. Li, Specific heat capacity improvement of molten salt for solar energy applications using charged single-walled carbon nanotubes, Appl. Energy 250 (2019) 1481–1490.
[15] MA Hassan, D. Banerjee, A soft computing approach for estimating the specific heat capacity of molten salt-based nanofluids, J. Mol. Liq. 281 (2019) 365–375.
[16] X Xiao, P Zhang, M. Li, Effective thermal conductivity of open-cell metal foams impregnated with pure paraffin for latent heat storage, Int. J. Therm. Sci. 81 (2014) 94–105.
[17] QQ Xiao, MD Zhang, JX Fan, L Li, T Xu, WH. Yuan, Thermal conductivity enhancement of hydrated salt phase change materials employing copper foam as the supporting material, Sol. Energy Mat. Sol. C 199 (2019) 91–98.
[18] CM Wang, TJ Wang, ZJ Hu, ZY. Cai, Facile synthesis and thermal performance of cety palmitate/nickel foam composite phase change materials for thermal energy storage, J. Energy Storage 28 (2020) 101179.
[19] P Zhang, X Xiao, ZN Meng, M. Li, Heat transfer characteristics of a molten-salt thermal energy storage unit with and without heat transfer enhancement, Appl. Energy 137 (2015) 758–772.
[20] ZF Wang, JN Wu, DQ Lei, H Liu, JP Li, ZY. Wu, Experimental study on latent thermal energy storage system with gradient porosity copper foam for mid-temperature solar energy application, Appl. Energy 261 (2020) 114472.
[21] R Cozzolino, D Chiappini, G. Bella, Experimental characterisation of a novel thermal energy storage based on open-cell copper foams immersed in organic phase change material, Energy Conver. Manage. 200 (2019) 112101.
[22] BVS Dinesh, A. Bhattacharya, Effect of foam geometry on heat absorption characteristics of PCM-metal foam composite thermal energy storage systems, Int. J. Heat Mass Tran. 134 (2019) 866–883.
[23] M Caliano, N Bianco, G Graditi, L. Mongibello, Analysis of a phase change material-based unit and of an aluminum foam/phase change material composite-based unit for cold thermal energy storage by numerical simulation, Appl. Energy 256 (2019) 113921.
[24] S Mousavi, A Kasaeian, MB Shafii, MH. Jahangir, Numerical investigation of the effects of a copper foam filled with phase change materials in a water-cooled photovoltaic/thermal system, Energy Conver. Manage. 163 (2018) 187–195.
[25] HJ Jouybari, S Saedodin, A Zamzamian, ME Nimvari, S. Wongwises, Effects of porous material and nanoparticles on the thermal performance of a flat plate solar collector: an experimental study, Renew. Energy 114 (2017) 1407–1418.
[26] QL Ren, FL Meng, PH. Guo, A comparative study of PCM melting process in a heat pipe-assisted LHTES unit enhanced with nanoparticles and metal foams by immersed boundary-lattice Boltzmann method at pore-scale, Int. J. Heat Mass Tran. 121 (2018) 1214–1228.
[27] JM Mahdi, EC. Nsofor, Solidification enhancement in a triplex-tube latent heat energy storage system using nanoparticles-metal foam combination, Energy 126 (2017) 501–512.
[28] JM Mahdi, EC. Nsofor, Melting enhancement in triplex-tube latent heat energy storage system using nanoparticles-metal foam combination, Appl. Energy 191 (2017) 22–34.
[29] JM Mahdi, HI Mohammed, ET Hashim, P Talebizadehsardari, EC. Nsoford, Solidification enhancement with multiple PCMs, cascaded metal foam and nanoparticles in the shell-and-tube energy storage system, Appl. Energy 257 (2020) 113993.
[30] X Xiao, HW Jia, DS Wen, XD. Zhao, Thermal performance analysis of a solar energy storage unit infiltrated with HITEC salt/copper foam composite seeded with nanoparticles, Energy 192 (2020) 116593.
[31] N Zhang, YP. Yuan, Synthesis and thermal properties of nanoencapsulation of paraffin as phase change material for latent heat thermal energy storage, Energy Built Environ. 1 (2020) 410–416.
[32] X Xiao, P. Zhang, Morphologies and thermal characterization of paraffin/carbon foam composite phase change material, Sol Energy Mat. Sol. C 117 (2013) 451–461.
[33] X Xiao, P. Zhang, Numerical and experimental study of heat transfer characteristics of a shell-tube latent heat storage system: part I – charging process, Energy 79 (2015) 337–350.
[34] X Xiao, G Zhang, YL Ding, DS. Wen, Rheological characteristics of molten salt seeded with Al_2O_3 nanopowder and graphene, Energies 12 (2019) 467.
[35] YW Hu, YR He, ZD Zhang, DS. Wen, Effect of Al_2O_3 nanoparticle dispersion on the specific heat capacity of a eutectic binary nitrate salt for solar power applications, Energy Convers. Manage. 142 (2017) 366–373.